Applied Surface Science 614 (2023) 156102

Contents lists available at ScienceDirect

Applied Surface Science

journal homepage: www.elsevier.com/locate/apsusc

Short communication

An exceptionally wear-resistant $CoFeNi_2$ medium entropy alloy via tribo-induced nanocrystallites with amorphous boundaries

Ao Meng [1], Fei Liang [1], Lei Gu, Qingzhong Mao, Yaping Zhang, Xiang Chen [*], Yonghao Zhao [*]

Nano and Heterogeneous Materials Center, School of Materials Science and Engineering, Nanjing University of Science and Technology, Nanjing 210094, China

ARTICLE INFO

Keywords:
Medium entropy alloy
Dry sliding
Subsurface microstructure evolution
TEM

ABSTRACT

Single-phase face centered cubic (FCC) high entropy alloys (HEAs) usually display high coefficients of friction and poor wear resistance at ambient temperature, especially for CoCrFeMnNi HEA and its derived CoCrFeNi and CoCrNi medium entropy alloys (MEAs). Here, we reported a novel $CoFeNi_2$ MEA exhibiting relatively low COFs (0.37–0.40); in particular, the wear rates (7.04×10^{-7} - 3×10^{-6} $mm^3\ N^{-1}\ m^{-1}$) are two orders of magnitude lower than the other derivatives. This is primarily due to the unexpected occurrence of topmost micrometer-thick layer consisting of sub-10 nm nanocrystallites surrounded by the amorphous boundaries during steady-stage sliding. This study ignites some insights into designing exceptional friction and wear resistant MEAs/HEAs by linking to tribo-induced surface deformation mechanisms.

1. Introduction

With the field of high entropy alloys (HEAs) coming to prominence in 2004 [1,2], the new concept can endow the alloys with good combination of strength and ductility [3,4], excellent fracture toughness [5,6] and remarkable work hardenability [7,8]. Besides, plenty of room left for the tribologists to explore the friction and wear behaviors of HEAs and their derived medium entropy alloys (MEAs), in an attempt to design novel wear-resistant alloys. However, single-phase face centered cubic (FCC) HEAs usually display low strength, high coefficients of friction (COF) and poor wear resistance at ambient temperature, especially for CoCrFeMnNi HEA and its derived CoCrFeNi and CrCoNi MEAs [9–15]. For instance, the CoCrFeMnNi HEA displayed a COF of 0.6 and wear rate of 3×10^{-4} $mm^3\ N^{-1}\ m^{-1}$ [13] and the CoCrFeNi MEA presented a COF of 0.74 and wear rate of 1.36×10^{-3} $mm^3\ N^{-1}\ m^{-1}$ [15] during dry sliding. The high COFs and large wear rates were entirely correlated to the brittleness of topmost nanocrystalline tribo-materials formed below the sliding surface. This stems from the very limited plastic deformation ability of nanocrystalline, triggering strain localization related surface roughening and cracking [16–18]. It is indicated that the mechanical stability and deformability of the tribo-materials is intimately related to the fate of the tribological contact [19,20].

From the viewpoint of materials science, some strategies were successfully attempted such as through compositional design forming a glaze layer aided by elevated temperature or self-organized ductile tribo-materials during sliding [11,13,21,22]. A protective glaze layer (compacted nanocrystalline oxides) was formed during dry sliding of the CoCrFeMnNi-based HEAs/MEAs above 200 °C, reducing the contact shear strength and thus bringing about substantial reduction in the COF and wear rates [11,13,21]. The other protective approach is to activate tribo-induced oxidation by adding proper elements for the in-situ formation of a hard and deformable amorphous-crystalline nanocomposite [22]. The nanocrystal aggregates were embedded in the amorphous matrix of the tribo-materials. It is therefore strongly suggested to induce such a ductile nanocomposite in an effort to enhance the tribological properties of HEAs/MEAs.

In this study, we attempt to investigate the CoFeNi MEA by avoiding Mn and Cr elements to achieve self-organized protection for friction and wear. Two reasons are as follows. The primary reason is that the oxide Mn_2O_3 and Cr_2O_3 were reported to be detrimental for protection, while cobalt-based oxide nanoparticles were verified to be wear resistant [23–25]. The decrease of Cr content was reported to reduce the COF of the CrCoNi MEA [26]. The second reason is that the beneficial amorphous structures were revealed to evolve from nano-lamellar structures during multiple sliding [23]. Concurrently, the CoFeNi MEA has relatively high stacking fault energy (SFE) about ~70 mJ m^{-2}, particularly favorable for the formation of lamellar structures through dislocation slip during sliding [27–29]. Moreover, the underlying friction and wear

* Corresponding authors.
E-mail addresses: xiang.chen@njust.edu.cn (X. Chen), yhzhao@njust.edu.cn (Y. Zhao).
[1] These authors contribute equally to this work.

https://doi.org/10.1016/j.apsusc.2022.156102
Received 8 November 2022; Received in revised form 4 December 2022; Accepted 14 December 2022
Available online 20 December 2022

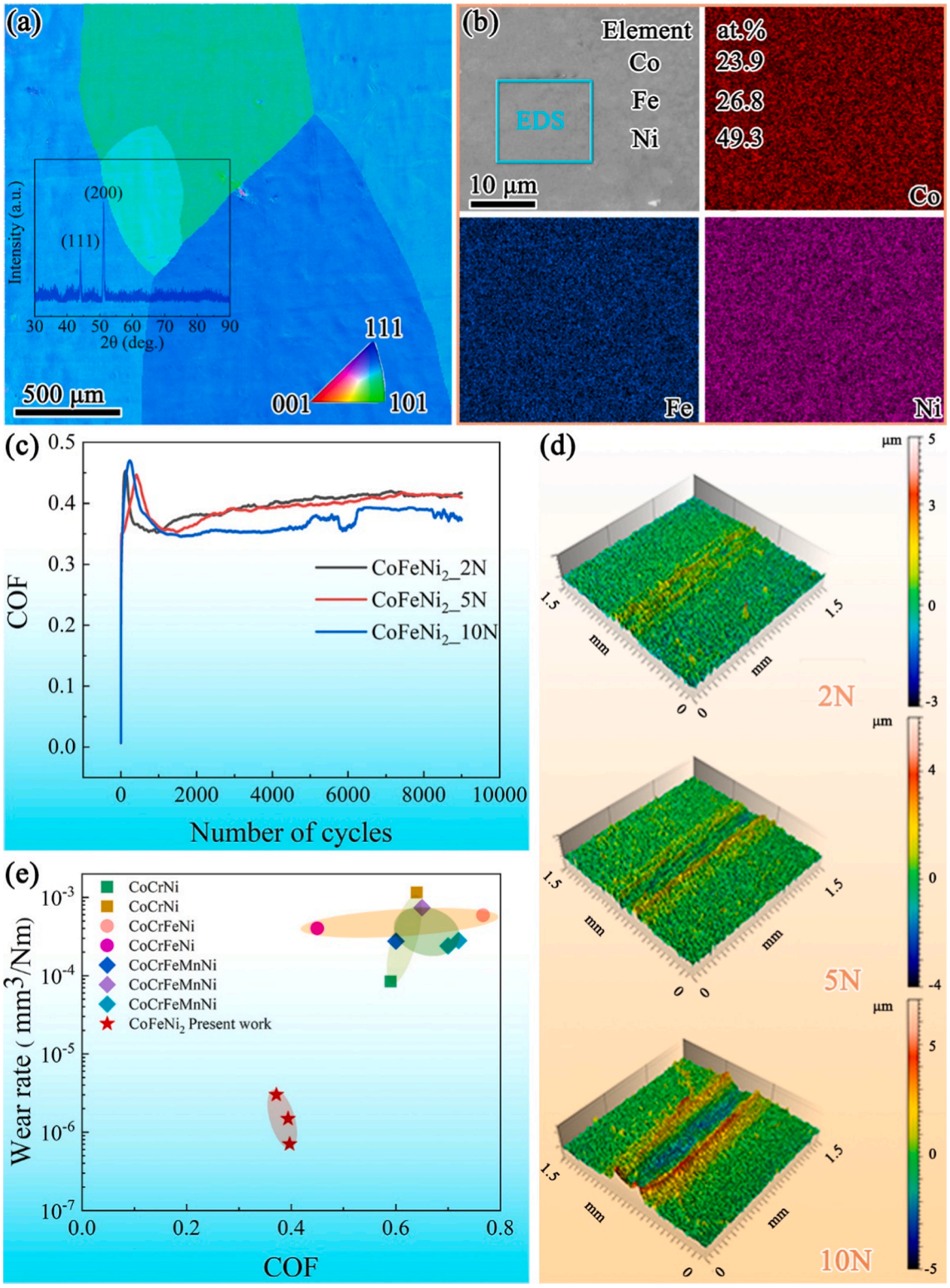

Fig. 1. Initial microstructures, compositional distributions and tribological characteristics of the as-cast $CoFeNi_2$ MEA. (a) EBSD orientation mapping of the alloy with XRD profiles and the orientation color code. (b) The SEM-EDS analysis of Co, Fe, and Ni elements and measured chemical compositions of the alloy. (c) COFs versus sliding cycles under different loads. (d) 3D profiles for surface morphologies of wear tracks at different loads. (e) Specific COF VS. wear rate maps of tribological CoCrFeMnNi-based HEAs/MEAs, including the present results of $CoFeNi_2$ MEA [10–15,30].

mechanisms will be disentangled by critically assessing tribo-induced structural and chemical changes and linking to stress field analysis.

2. Material and methods

The MEA ingots with a nominal composition of $CoFeNi_2$ (Co, Fe and Ni elements were employed with purities greater than 99.5 wt%) were fabricated by arc-melting in water-cooled copper crucible under the Ti-

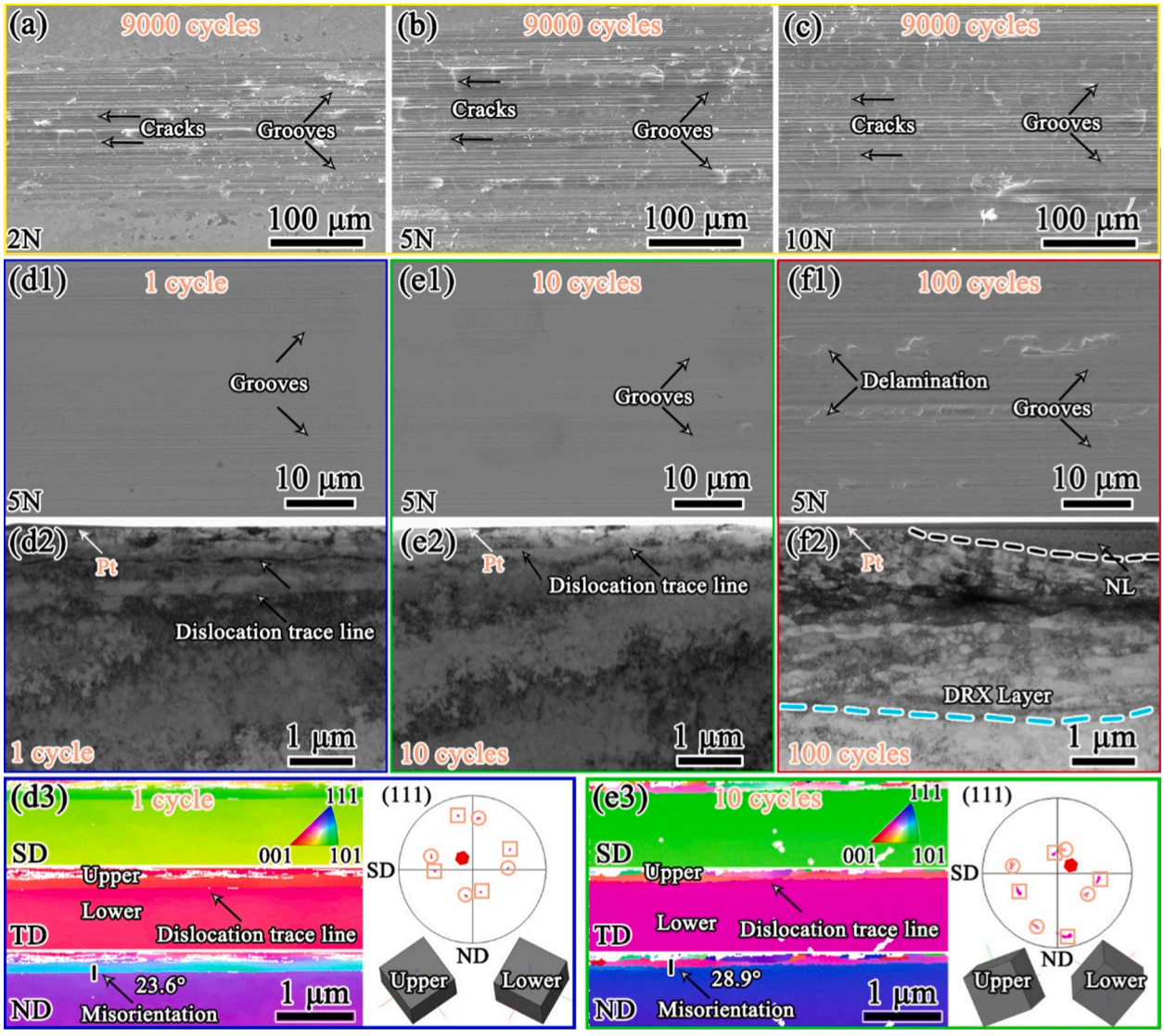

Fig. 2. SEM images of wear surfaces for the $CoFeNi_2$ MEA after 9000 sliding cycles at the various applied loads: (a) 2 N, (b) 5 N, (c) 10 N. SEM images of wear surfaces and corresponding TKD and TEM images for the FIB lifted ND-SD cross-sectional slices with the various cycles for the $CoFeNi_2$ MEA at 5 N: (d1-d3) 1 cycle, (e1-e3) 10 cycles, (f1-f2) 100 cycles. Note that the subsurface region between the two dislocation trace lines is termed as Upper and the matrix below the second dislocation trace line is termed as Lower. The SD-ND (111) pole figures for Lower (square) and Upper (circle) layers are plotted from Fig. 2d3 and e3, respectively. The common rotation axis is close to TD (hexagon).

gettered argon atmosphere. All ingots were flipped and re-melted several times to ensure the homogeneity of chemical composition. Cubic specimens with a dimension of 15 mm × 5 mm × 5 mm for friction tests were then sectioned from the ingots by electrical discharge machining. Prior to sliding, all specimens were mechanically grounded and then electropolished to be mirror-like. The Vickers hardness of $CoFeNi_2$ MEA was measured utilizing an HMV-G 21DT digital tester with a load of 980.7 mN and a loading time of 10 s. At least fifteen points were measured for each specimen. Reciprocating friction tests of the $CoFeNi_2$ MEAs were performed on an UMT-II tribometer (Bruker Co., Ltd., USA) in a ball-on-plate contact configuration. Dry conditions were selected at room temperature in air with a relative humidity of 45%, as shown in Fig.S1. Sapphire spheres with a diameter of 6 mm (Zhejiang Jienaier New Material Co., Ltd., China) were used as counter-bodies. The slide stroke was 2 mm. The normal loads were set as 2, 5 and 10 N and the sliding speed was kept as 10 mm s^{-1}. The COF values were recorded automatically and the wear rates were determined by measuring the profiles of the worn surfaces using a surface profilometer system (ASI Co, Ltd., USA). In addition, to uncover early surface deformation mechanisms, the sliding friction were interrupted after 1, 10 and 100 cycles at 5 N.

The electron back-scattered diffraction (EBSD) mapping of the as-casted ingots was obtained using a focused ion beam scanning electron microscope (FIB/SEM, Carl Zeiss-Auriga-45-66, Germany) equipped with automatic Oxford Instruments Aztec system. The microstructural characterization and chemical composition of the alloys were analyzed by a SEM (Quanta 250 F, FEI, USA) equipped with an Oxford X-Max energy dispersive X-ray Spectrometer detector (EDS). The normal direction-sliding direction (ND-SD) cross-sections of worn surfaces were prepared for transmission electron microscope (TEM) and transmission Kikuchi diffraction (TKD) by cutting in the middle of the wear track using a FIB system (Fig.S1). TEM (FEI-Tecnai G2 20 S-TWIN) at 200 kV and high-resolution transmission electron microscope (HRTEM, Titan G2 60–300 microscopes) in conjunction with EDS (Oxford Instruments Link Isis, UK) at 300 kV were employed to characterize the worn subsurface.

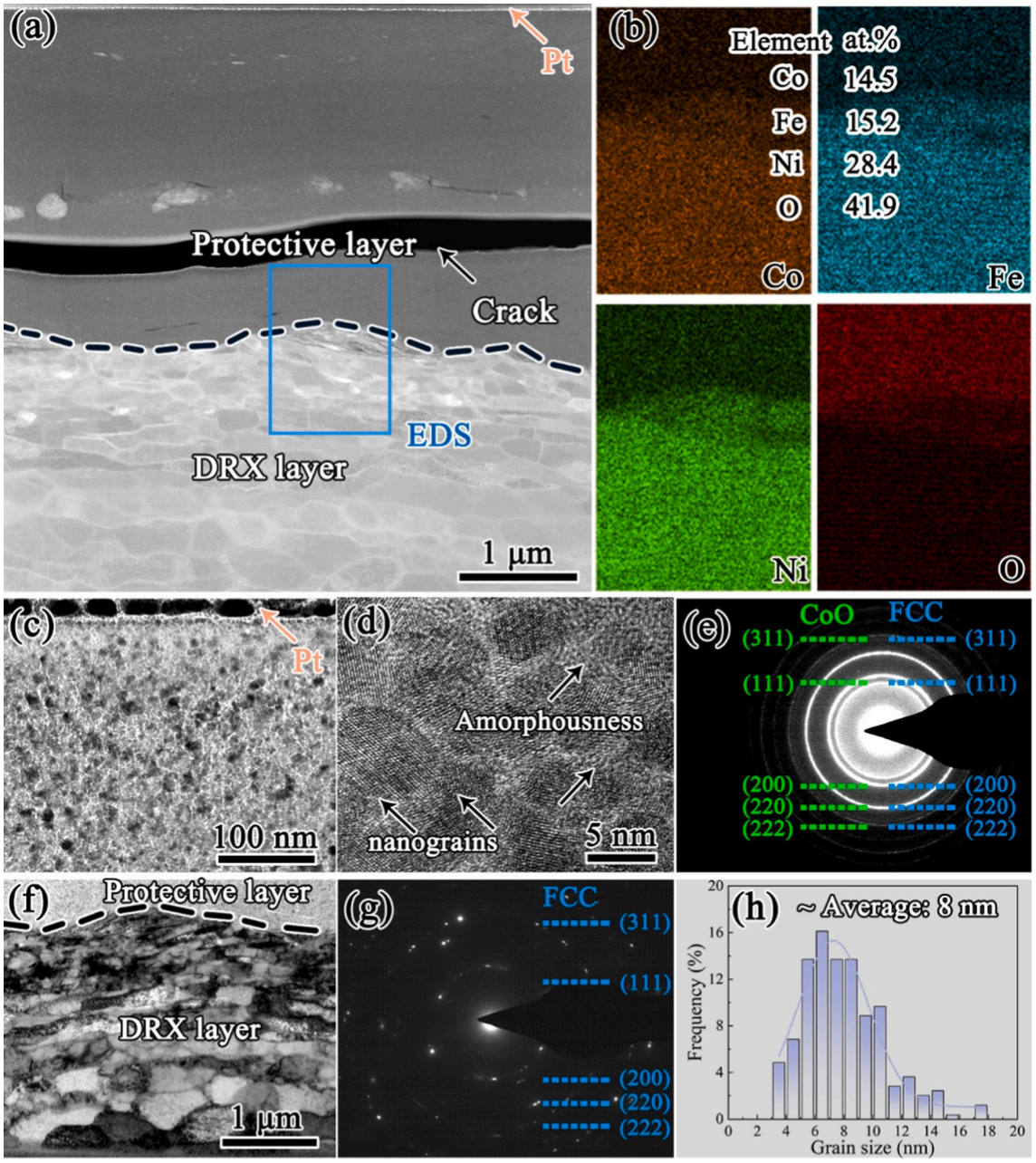

Fig. 3. (a) STEM image for the FIB lifted ND-SD cross-sectional slices with the 9000 cycles for the $CoFeNi_2$ MEA at 5 N. (b) The measured chemical compositions of the alloy from the selected blue rectangle in (a). (c) The TEM image of the topmost layer. (d-e) The corresponding HRTEM image and selected area electron diffraction (SAED) patterns for (c). (f-g) The detailed TEM image of DRX layer and corresponding SAED pattern. (h) The grain size distribution of the protective layer in the topmost. (For interpretation of the references to color in this figure legend, the reader is referred to the web version of this article.)

3. Results and discussion

The XRD pattern of the as-cast alloy (Fig. 1a) indicates a single-phase FCC structure. The initial microstructure of the alloy consists of coarse grains with several hundreds of micrometers in size with a hardness of 140.3 HV (Fig. 1a). The SEM-EDS elemental maps of the $CoFeNi_2$ alloy in Fig. 1b show that the distribution of Co, Fe, Ni appears to be uniform at the micrometer scale and the measured composition is close to the nominal one (see the inset of Fig. 1b). Fig. 1c shows the representative friction curves of the $CoFeNi_2$ MEA as a function of sliding cycles at various loads (2 N, 5 N and 10 N). The average COF of the $CoFeNi_2$ MEA is measured to be 0.40 at 2 N, slightly higher than those at 5 N (0.39) and 10 N (0.37). The 3D profiles for surface morphologies and representative ND-SD cross-sectional profiles of wear tracks show the discrepancy at different loads (Figs. 1d and S2). The width and depth increase with the increasing load. The shallow and narrow wear tracks of $CoFeNi_2$ MEA at room temperature are reflected by its low specific wear rates at different loads (2 N: 7.04×10^{-7} mm^3 N^{-1} m^{-1}, 5 N: 1.48×10^{-6} mm^3 N^{-1} m^{-1}, 10 N: 3×10^{-6} mm^3 N^{-1} m^{-1}). Fig. 1e plots the COFs and specific wear rates of the current $CoFeNi_2$ MEAs, compared with the reported CoCrFeMnNi-based MEAs/HEAs [10–15,30]. The $CoFeNi_2$ alloy shows lower COFs at room temperature. Besides, the average specific wear rates of the alloy lie in the magnitude of 10^{-6} mm^3 N^{-1} m^{-1}, two orders of magnitude lower than those of other MEAs/HEAs (10^{-3}–10^{-4} mm^3 N^{-1} m^{-1}).

The morphologies of the wear surfaces of $CoFeNi_2$ MEA at various loads are shown in Fig. 2a–c. After 9000 sliding cycles, the wear tracks display the similar morphologies i.e., abundant shallow grooves along

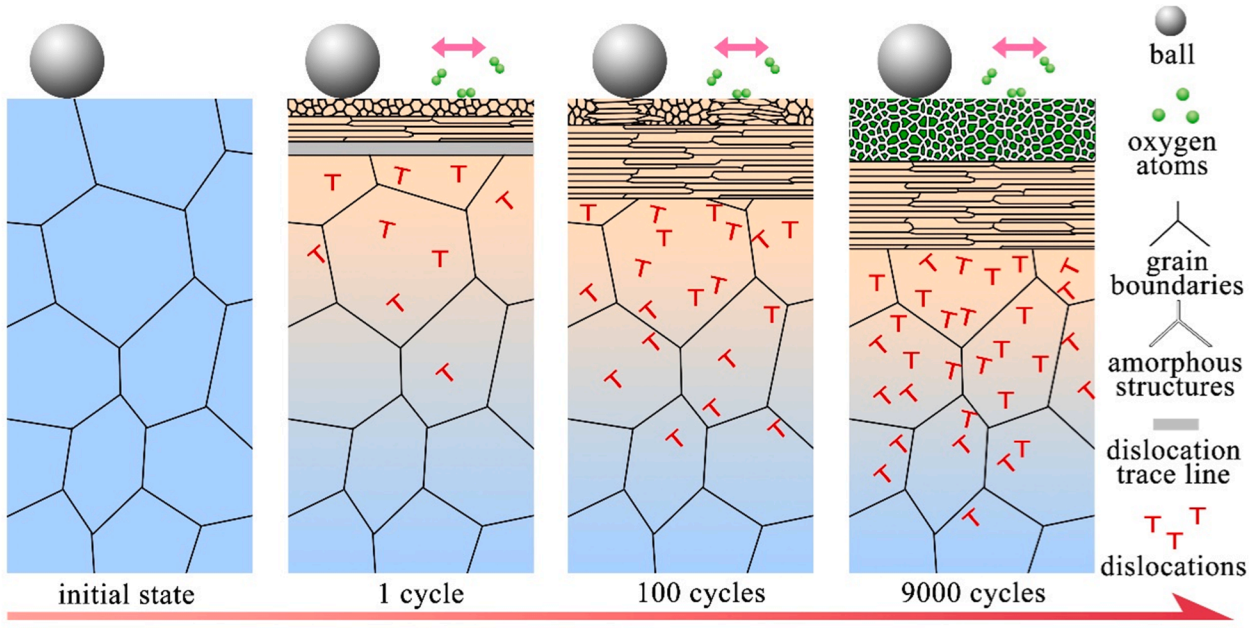

Fig. 4. Diagrams of the microstructural evolution of $CoFeNi_2$ MEA at different sliding stages.

the SD accompanied with some vertical cracks. Such grooves are indications of abrasive wear mechanism. In addition, the width of wear tracks and crack density increase with the incremental load (Fig. S3), which is consistent with the increasing wear rates. To reveal the friction-induced microstructure evolution, the wear surface and ND-SD cross-sectional subsurface microstructure after 1, 10 and 100 cycles at 5 N are illuminated in Fig. 2d–f. After 1 cycle, several superficial grooves are generated without cracking (Fig. 2d1). The subsurface structure consists of a nanostructured layer with a thickness of ~500 nm and two dislocation trace lines with depths of 500 nm and 1.1 μm parallel to the sliding surface (Fig. 2d2). TKD was implemented to further characterize the crystal orientation of the subsurface structure. The upper dislocation trace line shows sharp transition in crystallographic orientation of ~23.6° with respect to the lower one, with the rotation axis nearly parallel to TD according to the SD-ND (111) pole figure in Fig. 2d3. After 10 cycles, the wear track remains smooth and no crack is identified on the surface (Fig. 2e1). Similar nanostructured layer and dislocation trace lines are captured in the subsurface region with the transition in crystallographic orientation increasing to ~28.9° (Fig. 2e2-e3). With further increasing to 100 cycles, the parallel grooves and delamination morphologies are both observed (Fig. 2f1). The friction-induced microstructure consists of a wavy nanolaminate (NL) layer and a dynamic recrystallization (DRX) layer at the depth of 2.9 μm (Fig. 2f2). The NL layer is made of laminated grains with an average transverse size of ~3.7 nm (Fig. 2f2 and Figs. S4a-b). Besides, oxygen is hardly detectable in the NL and DRX layers through EDS element mapping (Figs. S4c-d).

Fig. 3 shows the subsurface structure under the wear surface after 9000 sliding cycles at 5 N and the detailed lift process is shown in Fig. S5. The cross-sectional region could be separated into the topmost layer and DRX layer according to the grain morphology contrast in the HAADF-STEM image (Fig. 3a). It is worth noted that the thickness of topmost layer increases up to ~2.9 μm during sliding dynamic evolution, thus termed as self-organized protective layer at this stage. Fig. 3b shows the EDS element mapping and quantitative chemical compositions of the selected area in Fig. 3a. It reveals that the protective layer is oxygen enriched which stems from the oxidation reaction during the long-term reciprocating sliding, while the DRX layer primarily consists of Co, Fe, and Ni elements. The topmost layer is composed of equiaxed nanograins with an average grain size of ~8 nm (Fig. 3c and Fig. 3h). The HRTEM images show the nanograins are separated by the relatively disordered regions, which could be considered as amorphous phase at isolated boundaries (Fig. 3d). The multiple rings in the corresponding selected area electron diffraction (SAED) pattern (Fig. 3e), confirm the existence of nanoscale trioxide grains and the formed oxides are mainly CoO. The DRX layer has a single FCC structure and two characteristic regions: nano-lamellae with a transverse size of ~ 98 nm in the top region followed by ultrafine-grains with an average grain size of ~ 324 nm (Fig. 3f-g).

Hence, fundamental friction-induced structural and chemical features are established for the current MEA with superior tribological properties (Fig. 4). The dislocation trace lines beneath a nanostructured layer are observed in the incipient stage, in analogy to that of pure copper under tribological loading [31]. The topmost layer then evolves into a discontinuous nanostructured mixing layer with adjacent laminate structure, under multiple tribological loading with high strains and strain gradients. In the late stage, a micrometer-thick and continuous tribo-layer consisting of nanocrystalline surrounded by the amorphous phase protect the topmost MEA from friction and wear losses, in contrast to the reported amorphous-crystalline nanocomposite.

As far as tribo-oxidation is concerned, the current study solves the cumbersome friction and wear issues present in single-phase CoCrFeMnNi HEAs by avoiding the brittle oxides such as Mn_2O_3 and Cr_2O_3. According to the Ellingham diagram [32], the formation of cobalt-based oxides is more stable relative to nickel and iron oxidation products, when comparing their Gibbs free energies at room temperature. This is substantiated by the SAED pattern of the tribo-oxides (Fig. 3e). Seemingly, Co is beneficial for the formation of compacted nanocrystalline oxides at room temperature due to the sufficiently adherent and better sintering ability, albeit normally reported during sliding at elevated temperatures [25].

It should be pointed out that the resultant sub-10 nm oxide surrounded by the amorphous structures is decisive for the remarkable friction and wear properties. First, the incorporation of oxygen atoms into the alloy will modify the atomic coordination with directed bond contributions and a large negative enthalpy of mixing [22], enhancing the glass-forming ability. Second, the disordered grain boundaries tend to transform into metastable amorphous states as the grain size is less than 10 nm [33,34]. Solid state amorphization were also frequently reported in severe plastic deformation such as HPT, dynamic impact and ultrahigh tribological loading [23,35,36]. Third, tribo-induced laminate

structure due to relatively high SFE is beneficial for the formation of amorphous phase, ascribed to extensive dislocation activities during tribological loading with high strain rates and strain gradients [33,35]. The nanolaminate structure were also reported in metals or alloys (e.g., Ni, Al and their alloys) with high SFEs subjected to surface mechanical grinding treatments [29].

4. Conclusion

In summary, a novel friction- and wear-resistant $CoFeNi_2$ MEA was designed and the underlying mechanisms were revealed by linking to the surface deformation mechanisms in different sliding stages. The $CoFeNi_2$ MEA exhibits much lower COFs (0.37–0.40) and wear rates (7.04×10^{-7} - 3×10^{-6} $mm^3\ N^{-1}\ m^{-1}$), in contrast to the CoCrFeMnNi HEA and other derivatives. This is through proper composition design and self-organized sub-10 nm nanocrystallites surrounded by the amorphous structures in response to tribological loading. At the early stage of sliding, the dislocation trace lines are observed beneath the sliding surface, evolving into a nanolaminate layer and a more refined DRX layer. The present study indicates the design guideline for wear resistant HEA/MEAs and their worn subsurface structure features as well.

CRediT authorship contribution statement

Ao Meng: Data curation, Investigation, Writing – original draft, Formal analysis, Methodology. **Fei Liang:** Data curation, Methodology, Writing – original draft. **Lei Gu:** Investigation. **Qingzhong Mao:** Software. **Yaping Zhang:** Investigation. **Xiang Chen:** Supervision, Writing – original draft, Writing – review & editing, Validation, Conceptualization, Funding acquisition. **Yonghao Zhao:** Supervision, Funding acquisition.

Declaration of Competing Interest

The authors declare that they have no known competing financial interests or personal relationships that could have appeared to influence the work reported in this paper.

Data availability

No data was used for the research described in the article.

Acknowledgements

The authors would acknowledge financial supports from the National Key Research and DevelopmentProgram of China (Grant No. 2021YFA1200203), National Natural Science Foundation of China (Grant No. 52001165, 51225102, and 51931003), Natural Science Foundation of Jiangsu Province, China (Grant No. BK20220965 and BK20200475), Jiangsu Funding Program for Excellent Postdoctoral Talent (Grant No. 2022ZB251), and the Fundamental Research Funds for the Central Universities (Grant No. 30919011405, 30921011215 and 30922010401). The authors are thankful for the technical support from Jiangsu Key Laboratory of Advanced Micro & Nano Materials and Technology, and SEM, TEM and EBSD experiments are performed at the Center of Analytical Facilities Nanjing University of Science and Technology.

Appendix A. Supplementary data

Supplementary data to this article can be found online at https://doi.org/10.1016/j.apsusc.2022.156102.

References

[1] J.W. Yeh, S.K. Chen, S.J. Lin, J.Y. Gan, T.S. Chin, T.T. Shun, C.H. Tsau, S.Y. Chang, Nanostructured high-entropy alloys with multiple principal elements: novel alloy design concepts and outcomes, Adv. Eng. Mater. 6 (2004) 299–303.
[2] B. Cantor, I.T.H. Chang, P. Knight, A.J.B. Vincent, Microstructural development in equiatomic multicomponent alloys, Mater. Sci. Eng. A 375 (2004) 213–218.
[3] X. Gao, Y. Lu, B. Zhang, N. Liang, G. Wu, G. Sha, J. Liu, Y. Zhao, Microstructural origins of high strength and high ductility in an $AlCoCrFeNi_{2.1}$ eutectic high-entropy alloy, Acta Mater. 141 (2017) 59–66.
[4] S.Q. Yuan, B. Gan, L. Qian, B. Wu, H. Fu, H.H. Wu, C.F. Cheung, X.S. Yang, Gradient nanotwinned CrCoNi medium-entropy alloy with strength-ductility synergy, Scr. Mater. 203 (2021), 114117.
[5] B. Gludovatz, A. Hohenwarter, D. Catoor, E.H. Chang, E.P. George, R.O. Ritchie, A fracture-resistant high-entropy alloy for cryogenic applications, Science 345 (2014) 1153–1158.
[6] M.-H. Tsai, J.-W. Yeh, High-entropy alloys: a critical review, Mater. Res. Lett. 2 (2014) 107–123.
[7] P. Shi, W. Ren, T. Zheng, Z. Ren, X. Hou, J. Peng, P. Hu, Y. Gao, Y. Zhong, P. K. Liaw, Enhanced strength-ductility synergy in ultrafine-grained eutectic high-entropy alloys by inheriting microstructural lamellae, Nat. Commun. 10 (2019) 489.
[8] X. Gao, Y. Lu, J. Liu, J. Wang, T. Wang, Y. Zhao, Extraordinary ductility and strain hardening of $Cr_{26}Mn_{20}Fe_{20}Co_{20}Ni_{14}$ TWIP high-entropy alloy by cooperative planar slipping and twinning, Materialia 8 (2019), 100485.
[9] C. Nagarjuna, H.-J. You, S. Ahn, J.-W. Song, K.-Y. Jeong, B. Madavali, G. Song, Y.-S. Na, J.W. Won, H.-S. Kim, S.-J. Hong, Worn surface and subsurface layer structure formation behavior on wear mechanism of CoCrFeMnNi high entropy alloy in different sliding conditions, Appl. Surf. Sci. 549 (2021), 149202.
[10] J. Miao, T. Guo, J. Ren, A. Zhang, B. Su, J. Meng, Optimization of mechanical and tribological properties of FCC CrCoNi multi-principal element alloy with Mo addition, Vacuum 149 (2018) 324–330.
[11] S. Pan, C. Zhao, P. Wei, F. Ren, Sliding wear of CoCrNi medium-entropy alloy at elevated temperatures: Wear mechanism transition and subsurface microstructure evolution, Wear 440-441 (2019), 203108.
[12] Y. Geng, J. Chen, H. Tan, J. Cheng, J. Yang, W. Liu, Vacuum tribological behaviors of CoCrFeNi high entropy alloy at elevated temperatures, Wear 456-457 (2020), 203368.
[13] J. Joseph, N. Haghdadi, K. Shamlaye, P. Hodgson, M. Barnett, D. Fabijanic, The sliding wear behaviour of CoCrFeMnNi and AlxCoCrFeNi high entropy alloys at elevated temperatures, Wear 428-429 (2019) 32–44.
[14] A. Ayyagari, C. Barthelemy, B. Gwalani, R. Banerjee, T.W. Scharf, S. Mukherjee, Reciprocating sliding wear behavior of high entropy alloys in dry and marine environments, Mater. Chem. Phys. 210 (2018) 162–169.
[15] L. Yang, Z. Cheng, W. Zhu, C. Zhao, F. Ren, Significant reduction in friction and wear of a high-entropy alloy via the formation of self-organized nanolayered structure, J. Mater. Sci. Technol. 73 (2021) 1–8.
[16] X. Chen, Z. Han, X.Y. Li, K. Lu, Lowering coefficient of friction in cu alloys with stable gradient nanostructures, Sci. Adv. 2 (2016), e1601942.
[17] X. Chen, R. Schneider, P. Gumbsch, C. Greiner, Microstructure evolution and deformation mechanisms during high rate and cryogenic sliding of copper, Acta Mater. 161 (2018) 138–149.
[18] A. Dollmann, A. Kauffmann, M. Heilmaier, C. Haug, C. Greiner, Microstructural changes in CoCrFeMnNi under mild tribological load, J. Mater. Sci. 55 (2020) 12353–12372.
[19] J. Li, L. Dong, X. Dong, W. Zhao, J. Liu, J. Xiong, C. Xu, Study on wear behavior of FeNiCrCoCu high entropy alloy coating on Cu substrate based on molecular dynamics, Appl. Surf. Sci. 570 (2021), 151236.
[20] F. Liang, X. Xu, P. Wang, Y. Zhang, Z. Han, X. Chen, Microstructural origin of high scratch resistance in a gradient nanograined 316L stainless steel, Scr. Mater. 220 (2022), 114895.
[21] Y. Cui, J.Q. Shen, S.M. Manladan, K.P. Geng, S.S. Hu, Wear resistance of FeCoCrNiMnAlx high-entropy alloy coatings at high temperature, Appl. Surf. Sci. 512 (2020), 145736.
[22] C. Liu, Z. Li, W. Lu, Y. Bao, W. Xia, X. Wu, H. Zhao, B. Gault, C. Liu, M. Herbig, A. Fischer, G. Dehm, G. Wu, D. Raabe, Reactive wear protection through strong and deformable oxide nanocomposite surfaces, Nat. Commun. 12 (2021) 5518.
[23] C.-H. Yin, Y.-L. Liang, Y. Liang, W. Li, M. Yang, Formation of a self-lubricating layer by oxidation and solid-state amorphization of nano-lamellar microstructures during dry sliding wear tests, Acta Mater. 166 (2019) 208–220.
[24] H. Kato, K. Komai, Tribofilm formation and mild wear by tribo-sintering of nanometer-sized oxide particles on rubbing steel surfaces, Wear 262 (2007) 36–41.
[25] A. Viat, A. Dreano, S. Fouvry, M.-I. De Barros Bouchet, J.-F. Henne, Fretting wear of pure cobalt chromium and nickel to identify the distinct roles of HS25 alloying elements in high temperature glaze layer formation, Wear 376–377 (2017) 1043–1054.
[26] J. Zhang, W. Li, R. Qin, P. Chen, Y. Liu, X. Liu, L. Gao, An atomic insight into the stoichiometry effect on the tribological behaviors of CrCoNi medium-entropy alloy, Appl. Surf. Sci. 593 (2022), 153391.
[27] X.L. An, H. Zhao, C.L. Chu, T. Dai, T. Lu, Z.H. Huang, C. Guo, P.K. Chu, Hall-Petch relationship and corrosion behavior of cold-rolled CoNiFe medium entropy alloy, J. Alloys Compd. 807 (2019), 151698.
[28] F. Ren, S.N. Arshad, P. Bellon, R.S. Averback, M. Pouryazdan, H. Hahn, Sliding wear-induced chemical nanolayering in Cu–Ag, and its implications for high wear resistance, Acta Mater. 72 (2014) 148–158.

[29] X.C. Liu, H.W. Zhang, K. Lu, Strain-induced ultrahard and ultrastable nanolaminated structure in nickel, Science 342 (2013) 337–340.
[30] A. Verma, P. Tarate, A.C. Abhyankar, M.R. Mohape, D.S. Gowtam, V.P. Deshmukh, T. Shanmugasundaram, High temperature wear in CoCrFeNiCux high entropy alloys: the role of Cu, Scr. Mater. 161 (2019) 28–31.
[31] C. Greiner, Z. Liu, R. Schneider, L. Pastewka, P. Gumbsch, The origin of surface microstructure evolution in sliding friction, Scr. Mater. 153 (2018) 63–67.
[32] Y. Yao, Z. Huang, L.A. Hughes, J. Gao, T. Li, D. Morris, S.E. Zeltmann, B. H. Savitzky, C. Ophus, Y.Z. Finfrock, Q. Dong, M. Jiao, Y. Mao, M. Chi, P. Zhang, J. Li, A.M. Minor, R. Shahbazian-Yassar, L. Hu, Extreme mixing in nanoscale transition metal alloys, Matter 4 (2021) 2340–2353.
[33] Y.H. Zhao, Thermodynamic model for solid-state amorphization of pure elements by mechanical-milling, J. Non-Cryst. Solids 352 (2006) 5578–5585.
[34] M.R. Jones, B.L. Nation, J.A. Wellington-Johnson, J.F. Curry, A.B. Kustas, P. Lu, M. Chandross, N. Argibay, Evidence of inverse hall-petch behavior and low friction and wear in high entropy alloys, Sci. Rep. 10 (2020) 10151.
[35] Y.B. Wang, X.Z. Liao, Y.H. Zhao, E.J. Lavernia, S.P. Ringer, Z. Horita, T. G. Langdon, Y.T. Zhu, The role of stacking faults and twin boundaries in grain refinement of a Cu–Zn alloy processed by high-pressure torsion, Mater. Sci. Eng. A 527 (2010) 4959–4966.
[36] S. Zhao, Z. Li, C. Zhu, W. Yang, Z. Zhang, D.E.J. Armstrong, P.S. Grant, R. O. Ritchie, M.A. Meyers, Amorphization in extreme deformation of the CrMnFeCoNi high-entropy alloy, Sci. Adv. 7 (2021) eabb3108.